Branching Corrected Mean Field Method for Nonadiabatic Dynamics

*Jiabo Xu and Linjun Wang**

Center for Chemistry of Novel & High-Performance Materials, and Department of Chemistry, Zhejiang University, Hangzhou 310027, China

ABSTRACT: When describing nonadiabatic dynamics based on trajectories, severe trajectory branching occurs when the nuclear wave packets on some potential energy surfaces are reflected while those on the remaining surfaces are not. As a result, the traditional Ehrenfest mean field (EMF) approximation breaks down. In this study, two versions of the branching corrected mean field (BCMF) method are proposed. Namely, when trajectory branching is identified, BCMF stochastically selects either the reflected or the non-reflected group to build the new mean field trajectory or splits the mean field trajectory into two new trajectories with the corresponding weights. As benchmarked in six standard model systems and an extensive model base with two hundred diverse scattering models, BCMF significantly improves the accuracy while retaining the high efficiency of the traditional EMF. In fact, BCMF closely reproduces the exact quantum dynamics in all investigated systems, thus highlighting the essential role of branching correction in nonadiabatic dynamics simulations of general systems.

Nonadiabatic dynamics have attracted substantial interest in the past decades. Many important phenomena in chemistry, physics, biology, and material sciences (e.g., proton transfer,[1,2] photoisomerization,[3,4] charge transport,[5,6] exciton dissociation,[7,8] and nonradiative energy relaxation[9,10]) all fall into the category of nonadiabatic dynamics. Compared with adiabatic dynamics, nonadiabatic dynamics involve strongly coupled electronic and nuclear motion, and thus are generally difficult to deal with theoretically. The fully quantum simulations give accurate description but are normally too expensive to carry out in complex systems. Comparatively, mixed quantum-classical dynamics (MQCD) methods are widely utilized due to the potentially good balance between efficiency and reliability. Nowadays, the Ehrenfest mean field (EMF),[11] Tully's fewest switches surface hopping (FSSH),[12] and their many variants have become the most popular approaches for nonadiabatic dynamics simulations in different fields.[13-20]

Both EMF and FSSH utilize the time-dependent Schrödinger equation (TDSE) to characterize the electronic wavefunction evolution.[11,12] Their major difference lies in the description of nuclear motion. In EMF, the nuclei evolve on a single effective potential energy surface (PES), which is obtained through averaging over all the electronic states and using the quantum populations as weights. In comparison, FSSH forces the nuclei to move on an active PES at any time and allows stochastic surface hops between PESs according to the nonadiabatic coupling. As a result, FSSH can take into account the different motion of nuclear wave packets (WPs) on different PESs. FSSH has shown higher reliability,[12,21,22] better detailed balance,[23-25] and the ability to describe both strong and weak polaronic effects,[26-28] implying that surface hops play an

important role in the great success of the trajectory surface hopping (TSH) approach for nonadiabatic dynamics simulations.

In the literature, decoherence correction has been extensively studied in the field of MQCD,[29,30] and many different algorithms have been proposed.[31-44] It is widely assumed that there is only one effective WP on each PES along a trajectory and the total wavefunction can be constructed on the basis of these WPs. As the WPs move with different speed and acceleration, their overlap gradually decays with time. Such decay of mixing has been widely utilized to define the decoherence rate as a function of force[31-33] or energy[34-36] differences between different PESs under frozen Gaussian[45] and short time approximations. Auxiliary WPs have also been introduced to explicitly propagate on the adiabatic PESs and certain criterions of their overlaps have been utilized to reset the wavefunction coefficients.[37,38] A more robust decoherence rate formula has also been derived by Subotnik and coworkers from the quantum Liouville equation.[39-41] When WP reflection happens, however, the overlap between the relevant WPs decays rapidly within a very short period, preventing the definition of a standard decoherence rate. Recently, we have proposed the branching corrected surface hopping (BCSH) method, which deals particularly with the trajectory branching due to WP reflection without using decoherence rates.[42] As benchmarked in a series of standard model systems, BCSH reproduces almost the exact quantum results, indicating the important role of branching correction in TSH simulations.

In this work, a branching corrected mean field (BCMF) method is presented. We show that BCMF also gives very good description of nonadiabatic dynamics in standard

model systems and an additional model base consisting of two hundred diverse models. Actually, the accuracy of BCMF is as high as that of BCSH. Thereby, we show that making stochastic surface hops does not seem to be always essential while the proposed branching correction has universal significance in MQCD simulations.

We start with the traditional EMF approach to simulate a general system consisting of both nuclear and electronic degrees of freedom, whose coordinates are **R** and **r**, respectively. The total system Hamiltonian is expressed as

$$\hat{H} = \hat{T}_{\mathbf{R}} + \hat{T}_{\mathbf{r}} + \hat{V}(\mathbf{r},\mathbf{R}), \tag{1}$$

where $\hat{T}_{\mathbf{R}}$ and $\hat{T}_{\mathbf{r}}$ are nuclear and electronic kinetic energy operators, and $\hat{V}(\mathbf{r},\mathbf{R})$ covers all relevant interactions. Usually, we rewrite the Hamiltonian as

$$\hat{H} = \hat{T}_{\mathbf{R}} + \hat{H}_0(\mathbf{r},\mathbf{R}), \tag{2}$$

where $\hat{H}_0(\mathbf{r},\mathbf{R}) = \hat{T}_{\mathbf{r}} + \hat{V}(\mathbf{r},\mathbf{R})$ denotes the electronic Hamiltonian for fixed nuclear coordinates **R**. The electronic subsystem at a given time *t* is described quantum mechanically by the wavefunction, $|\psi(\mathbf{r},t)\rangle$, and the evolution follows the TDSE,

$$i\hbar \frac{\partial |\psi(\mathbf{r},t)\rangle}{\partial t} = \hat{H}_0\left(\mathbf{r},\mathbf{R}(t)\right)|\psi(\mathbf{r},t)\rangle . \tag{3}$$

The nuclear motion is governed by the classical Newton equation through the gradient of the expectation value of the system energy,[11]

$$\frac{\partial \mathbf{P}}{\partial t} = -\nabla_{\mathbf{R}} \langle \psi(\mathbf{r},t)| \hat{H}_0\left(\mathbf{r},\mathbf{R}(t)\right)|\psi(\mathbf{r},t)\rangle , \tag{4}$$

where **P** are the nuclear momenta. The EMF simulation of nonadiabatic dynamics is realized through iteratively solving the combined Eqs. (3) and (4).

EMF can be viewed as the classical limit of the time-dependent self-consistent field

(TDSCF) theory[46,47] and can also be derived from the mixed quantum-classical Liouville (MQCL) equation.[48,49] Following the traditional picture of TDSCF, the total nuclear-electronic wavefunction is approximately factorized as[46]

$$\left|\Psi(\mathbf{r},\mathbf{R},t)\right\rangle = \left|\psi(\mathbf{r},t)\right\rangle\left|\chi(\mathbf{R},t)\right\rangle \exp\left[\frac{i}{\hbar}\int_0^t E_0(t')dt'\right]. \tag{5}$$

Here, $\left|\psi(\mathbf{r},t)\right\rangle$ and $\left|\chi(\mathbf{R},t)\right\rangle$ are electronic and nuclear wavefunctions at time t, and $E_0(t)$ is a phase factor. Apparently, the nuclear WPs on different PESs are approximated by an effective WP in the traditional EMF approach. To go beyond this approximation, we return to the original picture, that is, there exists one WP component on each PES. For the sake of simplicity and without loss of generality, we consider only one classical degree of freedom and two electronic levels hereafter unless otherwise noted. However, the approach can be easily generalized to more complex systems. As shown in Figs. 1A, 1B, and 1C, an effective WP with coordinate **R** is assumed to provide a good description of the system. Thus, all the WP components approximately locate at the same position **R**. The momentum of the WP on the ith PES, $\mathbf{P}_i$, can be obtained based on the assumptions of parallel momenta and energy conservation,

$$\mathbf{P}_i = \eta\mathbf{P}\,, \tag{6}$$

$$\frac{\mathbf{P}_i^2}{2m} + E_i = \frac{\mathbf{P}^2}{2m} + E_{avg}\,. \tag{7}$$

Here, **P** is the momentum of the effective WP, η is a positive number to be solved, m is the nuclear mass, E_i and E_{avg} are energy of the ith PES and the average potential energy at coordinate **R**. Following previous studies,[42] $\mathbf{P}_i$ is set to be positive infinitesimal when Eq. (7) cannot be fulfilled.

If we focus only on the position and momentum, WP dynamics on a PES can be reasonably described by the corresponding Newton equation. Apparently, the EMF approximation works well when the WP trajectories on different PESs are similar. When they branch in the phase space, however, one effective WP cannot represent the overall behavior anymore and additional corrections are necessary. The most significant mechanism of trajectory branching is associated with WP reflection.[42] As shown in Fig. 1, there exist three different types of WP branching in the mean field picture. When the WPs on some adiabatic PESs are reflected (see Figs. 1D and 1E), their trajectories become considerably different with those of other WPs. Using the original effective WP (see Figs. 1A and 1B) as a reference, we may classify the quantum states into two subgroups: one RG group with reflected WPs and one NRG group with non-reflected WPs in general multilevel systems. The WPs of the two groups separate quickly and soon become decoupled. As a result, the traditional TDSE in Eq. (3) also breaks down. In these circumstances, each of the RG and NRG groups should be described by their own effective WP after WP branching within the mean field machinery (see Figs. 1G and 1H). Besides these two major types, there also exists a special case where the WPs on all adiabatic PESs are not reflected but the effective WP is reflected (see Fig. 1F). Hereby, the effective WP also becomes incapable of describing the nuclear motion. As shown in Fig. 1I, the mean field trajectory should be adjusted accordingly.

The WP components on different PESs propagate with different momenta, and thus they accumulate different phases with time. Using the traditional TDSE results in inconsistency concerning the phase evolution. In the framework of FSSH, a phase

correction approach has been proposed by Shenvi and coworkers.[50] Here, we extend it to the mean field approach. At nuclear position **R**, the electronic eigenstates, $\left|\phi_i(\mathbf{r};\mathbf{R})\right\rangle$, and eigenenergies, $E_i(\mathbf{R})$, are obtained through solving

$$\hat{H}_0(\mathbf{r},\mathbf{R})\left|\phi_i(\mathbf{r};\mathbf{R})\right\rangle = E_i(\mathbf{R})\left|\phi_i(\mathbf{r};\mathbf{R})\right\rangle . \tag{8}$$

The electronic wavefunction is then expanded as a linear combination of $\left|\phi_i(\mathbf{r};\mathbf{R}(t))\right\rangle$,

$$\left|\psi(\mathbf{r},t)\right\rangle = \sum_i c_i(t)\left|\phi_i\left(\mathbf{r};\mathbf{R}(t)\right)\right\rangle, \tag{9}$$

where $c_i(t)$ are the wavefunction coefficients. Substituting Eq. (9) to Eq. (3) yields

$$i\hbar\frac{dc_i}{dt} = \sum_j H_{ij}c_j , \tag{10}$$

where the electronic Hamiltonian elements are given by

$$H_{ij} = E_i\delta_{ij} - \frac{i\hbar\mathbf{P}\cdot\mathbf{d}_{ij}}{m} . \tag{11}$$

Here, $\mathbf{d}_{ij} = \left\langle\phi_i(\mathbf{r};\mathbf{R})\right|\nabla_{\mathbf{R}}\left|\phi_j(\mathbf{r};\mathbf{R})\right\rangle$ are the nonadiabatic coupling (NAC) vectors. Suppose the NACs are negligible, the WPs on different adiabatic PESs evolve independently with time. Then, the following effective Hamiltonian can be defined,[50]

$$H_{ij}^{eff} = -\frac{\mathbf{P}\cdot\mathbf{P}_i}{m}\delta_{ij} - \frac{i\hbar\mathbf{P}\cdot\mathbf{d}_{ij}}{m} , \tag{12}$$

and used to replace the original Hamiltonian in Eq. (11) for wavefunction propagation with the correct phase difference between the WP components. Note that a similar phase correction approach has also been derived by Zhu in a different perspective based on the conventional time-independent semiclassical phase integral.[51]

In BCMF calculations, a number of independent realizations are carried out with an initial sampling similar to that used in the classical Wigner approximation.[52,53]

Namely, the nuclear coordinates and momenta at time zero are sampled from the Wigner distribution of the initial nuclear wavefunction. The step-by-step outline of our BCMF algorithm with stochastic wavefunction collapse (BCMF-s) is as follows:

(1) At each time step t, the nuclear coordinate $\mathbf{R}(t)$ and momentum $\mathbf{P}(t)$ are updated by solving Eq. (4), and the electronic wavefunction $\left|\psi(\mathbf{r},t)\right\rangle$ is propagated according to Eq. (3) with the effective electronic Hamiltonian given by Eq. (12).

(2) The momenta of all WP components are calculated by Eqs. (6) and (7). For each adiabatic PES i, we further obtain the nuclear momentum at time $t + \Delta t$ with $\mathbf{P}_i(t + \Delta t) = \mathbf{P}_i(t) + \mathbf{F}_i(t)\Delta t$, where $\mathbf{F}_i$ is the corresponding Hellmann-Feynman force. If the dot products $\mathbf{F}_i(t)\cdot\mathbf{P}_i(t)$ and $\mathbf{F}_i(t)\cdot\mathbf{P}_i(t + \Delta t)$ have different signs, a WP reflection event is supposed to take place on the ith PES during the time interval Δt. Similarly, for the average PES, the momentum of the effective WP at time $t + \Delta t$ is calculated by $\mathbf{P}(t + \Delta t) = \mathbf{P}(t) + \mathbf{F}_{avg}(t)\Delta t$, where $\mathbf{F}_{avg}$ is the mean field nuclear force. If $\mathbf{F}_{avg}(t)\cdot\mathbf{P}(t)$ and $\mathbf{F}_{avg}(t)\cdot\mathbf{P}(t + \Delta t)$ differ in sign, the effective WP is reflected on the average PES.

(3) When WP reflection happens, different corrections are implemented depending on the nature of trajectory branching. In the first and second types, some of the WPs on adiabatic PESs get reflected while the others do not. Here, we classify all the quantum states into a RG subgroup with reflected WPs and a NRG subgroup with non-reflected WPs, and randomly choose one of them based on their electronic populations, i.e., $P_{RG} = \sum_{i\in RG} |c_i|^2$ and $P_{NRG} = \sum_{i\in NRG} |c_i|^2$. Namely, a uniform random number $\xi \in (0, 1)$ is generated. If $\xi < P_{RG}$, the RG group is chosen, and we reset the wavefunction coefficients to $c'_{i\in NRG} = 0$ and $c'_{i\in RG} = c_i / P_{RG}^{1/2}$; Otherwise, the NRG group is chosen,

and we reset $c'_{i\in RG}=0$ and $c'_{i\in NRG}=c_i/P_{NRG}^{1/2}$. Then, the average PES is modified, and the nuclear momentum of the effective WP is rescaled to conserve the total energy,

$$\mathbf{P}'(t)=\mathbf{P}(t)\sqrt{1+\frac{E_{avg}-E'_{avg}}{\mathbf{P}(t)^2/2m}}, \tag{13}$$

where E_{avg} and E'_{avg} are the averaged energies before and after the branching correction. If this energy conservation is violated, the other energetically accessible group is chosen instead. Especially, it is possible that a WP satisfies energy conservation at time t - Δt and gets reflected during [t - Δt, t], but the energy conservation does not hold at time t. Apparently, a WP branching event should be identified in this case and $\mathbf{P}'(t)$ is simply reset to zero. In the third type, the effective WP gets reflected while the WPs on all the adiabatic PESs are not. Then, we construct a new mean field PES with only energetically allowed states. Namely, we reset the wavefunction coefficients of the energy-forbidden states to zero and renormalize the total electronic wavefunction. The nuclear momentum is also adjusted by Eq. (13).

(4) Repeat steps (1)-(3) until a predefined criterion is satisfied. To properly describe the asymptotic region, the electronic wavefunction is transformed taking the energy conservation into account. Namely, the wavefunction coefficients of the energy-forbidden states are reset to zero and the then the wavefunction is renormalized. Finally, the electronic population on the ith state is calculated by $P_i=\sum_j|c_i^{(j)}|^2$, where $c_i^{(j)}$ is the ith transformed electronic coefficient of the jth trajectory.

BCMF can also be realized by means of a trajectory splitting algorithm. Namely, when the first or the second type of trajectory branching happens, the parent trajectory

is split into two child trajectories, which represent the reflected and non-reflected WPs, respectively. Each trajectory is associated with a weighting factor corresponding to its probability (i.e., P_{RG} or P_{NRG}). We refer this algorithm as BCMF based on weights (BCMF-w). Unlike BCMF-s with only one trajectory explicitly propagated in each realization, all the branched trajectories are propagated simultaneously in BCMF-w. The detailed algorithm is given in the Supporting Information (SI). Note that the two BCMF approaches are intrinsically identical to each other as will be discussed below. In the following studies, we use the BCMF-s algorithm unless otherwise noted.

To systematically benchmark the performance of BCMF, we study a series of one-dimensional two-level scattering models. We first consider six well-studied systems in the literature,[12,39,51] namely, the simple avoided crossing (SAC), the dual avoided crossing (DAC), the extended coupling with reflection (ECR), the dumbbell geometry (DBG), the double arch geometry (DAG), and the dual Rosen-Zener-Demkov non-crossing (DRN) models. The PESs and NACs are shown in Fig. S1 of the SI. For each model, there exist four reaction channels, i.e., transmission and reflection on the lower and upper PESs. The fully quantum solutions obtained by the discrete variable representation (DVR) method with absorbing potentials are adopted as references.[54,55] In Figs. 2A-2F, we focus on only one major channel per model. The computational details and results of all relevant channels are provided in the SI.

In Figs. 2A and 2B, we show transmission populations on the upper surfaces as a function of the initial nuclear momentum in the SAC and DAC models. As shown in Figs. S1A and S1B, WPs can be temporally trapped in the potential wells on the upper

PESs, oscillating and spawning child WPs to the lower surfaces. As WP branching is completely neglected in the traditional EMF, the reflected channels are absent in both models (see Figs. S2 and S3 in the SI). In the meanwhile, the transmission populations of EMF are larger than the quantum solutions for small k (see Figs. 2A and 2B). The problem can be solved after the implementation of our branching and phase corrections, and the results of BCMF agree very well with the exact quantum solutions.

Figs. 2C and 2D show the reflection populations on the lower PESs of ECR and DBG models, which have been extensively studied due to their significant decoherence effects. Namely, when the incoming WP reflects on the upper PES, it quickly becomes separated and decoupled with the WP on the lower PES, leading to clear quantum decoherence. Due to the failure in describing WP branching, EMF gives totally wrong reflection results for the ECR model and the large momentum region in the DBG model. Actually, the EMF description of ECR and DBG models is generally much worse than that in the SAC and DAC models (see Figs. S4 and S5). In comparison, BCMF naturally reproduces the quantum solutions in all channels.

In Figs. 2E and 2F, the momentum-dependent transmission populations on the upper surfaces of DAG and DRN models are given. These two models are more complex as they require highly balanced description of coherence and decoherence. In the DAG model, the exact results are smooth for small k and oscillatory for large k. With similar PESs, however, DRN shows irregular weak oscillations in the quantum dynamics. Without decoherence, EMF fails to describe the transmission in the small k region (see Figs. 2E and 2F) and the reflection channels (see Figs. S6 and S7) in both

models. Again, the BCMF results are almost on top of the exact quantum solutions in all cases, which further proves the reliability of BCMF in dealing with complex systems.

The main difference between BCMF-s and BCMF-w lies in their computational cost instead of the accuracy. To illustrate this, we calculate the average population deviations based on the results of the six standard models investigated above,

$$\sigma_n = \sqrt{\frac{1}{N}\sum_{i=1}^{N}\left(P_i^n - P_i^0\right)^2}\,. \tag{14}$$

Here, P_i^n is the value of ith data point calculated by either BCMF-s with n trajectories or BCMF-w with one realization containing at most n trajectories, and P_i^0 represents the corresponding converged value. Each data point refers to the population of a specific channel, i.e., transmission or reflection on the lower or upper surface in one of the six models at a given k. In total, the number of data points considered here is $N = 1156$. To eliminate the statistical error due to the initial Wigner sampling, the coordinates and momenta at time zero are simply assigned as their mean values here. In Fig. 3A, we show the average population deviations with different numbers of trajectories by the two BCMF algorithms. Apparently, BCMF-w converges faster due to its non-stochastic nature. Reliable results can already be achieved by a few tens of branched trajectories, which are approximately two orders of magnitude less than those required in BCMF-s. In Fig. 3B, we systematically compare the converged results of the 1156 data points calculated by BCMF-w and BCMF-s. All the data points are almost on the diagonal line, indicating that the two BCMF algorithms are intrinsically identical.

In BCMF-w, new trajectories are spawned whenever WP branching happens, and

all the branched trajectories are propagated simultaneously. Thereby, for systems where WP branching occurs frequently, such as the DAC model with a potential well on the upper surface, relatively larger number of trajectories are required to characterize the frequent trajectory splitting. In general, each BCMF-w realization requires a higher cost of memory, but the demand for realizations is significantly reduced. As a comparison, though more realizations are needed in BCMF-s, trajectories can be parallelly simulated to reduce the memory cost and increase the numerical efficiency, thus more promising for long-time simulations of complex systems. When the number of branches becomes enormous, BCMF-s can also benefit substantially from its stochastic feature.

The robustness of BCMF is further benchmarked in an extensive model base, which contains 200 diverse scattering models with two quantum levels and one classical degree of freedom. The model Hamiltonians and computational details are given in the SI. Here, 20800 channel populations are relevant as we consider 26 different nuclear momenta and 4 transmission/reflection channels per model. In Figs. 4A and 4B, we compare the exact solutions by DVR and the results by EMF and BCMF, respectively. The degree of proximity of these data points to the diagonal line indicates the accuracy of the corresponding method. As shown in Fig. 4A, the traditional EMF exhibits a wide distribution with a large number of data points obviously far away from the diagonal line. In contrast, most of the BCMF results agree excellently with the exact solutions (see Fig. 4B), and only a few data points exhibit relatively large errors (as highlighted in red). We find that these data points correspond to five calculations, all of which share a common feature: the total energy is close to the maximum energy of the lower PES

(see Figs. S9-S13 in the SI). We know that the classical Wigner approximation cannot properly describe such strong nuclear quantum effects in adiabatic dynamics. In BCMF, we consider similar Wigner sampling at time zero and classical dynamics in the following dynamics simulations, and thus the data points with the largest errors in BCMF are most probably due to similar nuclear quantum effects. Except these special cases, the reliability of all BCMF calculations in the whole model base is generally very high (see Fig. 4B), which is encouraging.

To quantify the performances of EMF and BCMF, we further study the error distribution of the 20800 channel populations. As shown in Fig. 5A, 97% of the data points show errors less than 0.01 with BCMF, while the percentage is only 72% with the traditional EMF. Moreover, the error distribution of BCMF is much narrower than that of EMF. About 8% of the data points by EMF exhibit errors larger than 0.1. In contrast, this ratio is only 1‰ in BCMF, which has been reduced by almost two orders of magnitude. For a given initial k, the average population error σ is defined as

$$\sigma = \sqrt{\frac{1}{800}\sum_{n=1}^{200}\sum_{i=1}^{4}\left(P_{ni}^{MF} - P_{ni}^{Exact}\right)^2}, \tag{15}$$

where P_{ni}^{MF} and P_{ni}^{Exact} are populations of the ith transmission or reflection channel in nth model calculated by a mean field method and the exact quantum dynamics, respectively. In Fig. 5B, we show the momentum-dependent average population errors of EMF and BCMF. To reveal the intrinsic performances, we also exclude the channels associated with strong nuclear quantum effects mentioned above. The average population errors are recalculated and labeled as EMF* and BCMF* in Fig. 5B. For the

standard EMF, the error is about 0.1 for small k and gradually reduces to 0.02 for large k. The EMF errors are so large that the performance of EMF* remains almost the same. In contrast, the average population errors of BCMF are significantly reduced. Especially, the errors are negligible in the large k region. Note that these results are very close to those by the BCSH method proposed recently.[42] When the channels with strong quantum effects are removed, the average population errors for small k are evidently reduced and the momentum dependence becomes even smoother. The average errors of BCMF* are all less than 0.015 and decrease monotonously with k. The about 10-fold improvement of accuracy over the traditional EMF emphasizes the significance of branching correction in mean field dynamics and MQCD in general.

In summary, we have proposed a novel BCMF approach for nonadiabatic dynamics simulations with the wavefunction propagation taking WP branching and phase difference into account. WP reflection has been identified as the main mechanism that leads to the breakdown of the traditional EMF approximation. Three types of trajectory branching (i.e., the effective WP is reflected or non-reflected when WPs on some adiabatic PESs are reflected, and the effective WP gets reflected while WP components on all adiabatic PESs do not) have been studied, and corrections to the mean field trajectory have been introduced accordingly. Two BCMF algorithms (i.e., BCMF-w and BCMF-s) have been presented, and it has been shown that they give the same converged results and different computational advantages in different cases. As demonstrated in a series of standard and additional scattering problems, BCMF has shown significant advantages regarding both the average error and the error distribution, while holding

the simple formalism and low computational cost of the traditional EMF method. Considering the encouraging performance, BCMF has great potential to achieve a better balance of reliability and efficiency in general applications.

Finally, there are still a few points that worth discussing. (1) Compared with the mean field approach, surface hopping has long been recognized as a more reliable framework for MQCD.[12,15,46] On the basis of the present study, BCMF can also provide highly reliable results with accuracy comparable to BCSH, and thus it seems that a proper description of WP branching is more essential in MQCD. The current algorithm of branching correction is based solely on WP reflection, more sophisticated judgement and treatment of WP branching may be required in further studies. (2) Multiple spawning is another popular method to simulate nonadiabatic dynamics.[56,57] There, new WPs are generated in the interaction region with large NACs. In our BCMF, however, new trajectories are generated when WP branching takes place and the branched WPs are still characterized in a mean field manner. Note that another branching criterion was recently proposed by Shi and coworkers[49] and may be useful to further improve the performance of BCMF. (3) Previous studies show that the mean field approach can automatically characterize the Berry phase[58,59] and naturally treat trivial crossings,[15,19] while traditional surface hopping does not.[60-65] This also justifies the urgent demand to develop robust mean field methods like BCMF. Developing BCMF variants to deal with the Berry phase and trivial crossings in complex systems deserves further study. (4) In some sense, the present BCMF algorithm for nonadiabatic dynamics is analogous to the classical Wigner approximation for adiabatic dynamics.[52,53] Both approaches

benefit from the initial Wigner sampling to consider most of the nuclear quantum effects. When strong nuclear quantum effects emerge, however, better semiclassical dynamics approaches may be useful.[66,67] (5) To get reliable populations in the asymptotic region, BCMF resets wavefunction coefficients considering the energy conservation. Note that similar algorithms have been utilized in the Liouville space surface hopping.[68,69] A slow decoherence effect due to traditional decay of mixing may be responsible for this.[31-36] Relevant studies are currently under way.

ASSOCIATED CONTENT

Supporting Information

Computational details and more numerical results. This material is available free of charge online.

AUTHOR INFORMATION

Corresponding Author

*E-mail: ljwang@zju.edu.cn.

Notes

The authors declare no competing financial interests.

ACKNOWLEDGMENTS

We thank Professor Zhenggang Lan and Professor Jiushu Shao for helpful discussions. L.W. acknowledges the National Natural Science Foundation of China (Grant Nos. 21922305, 21873080, and 21703202).

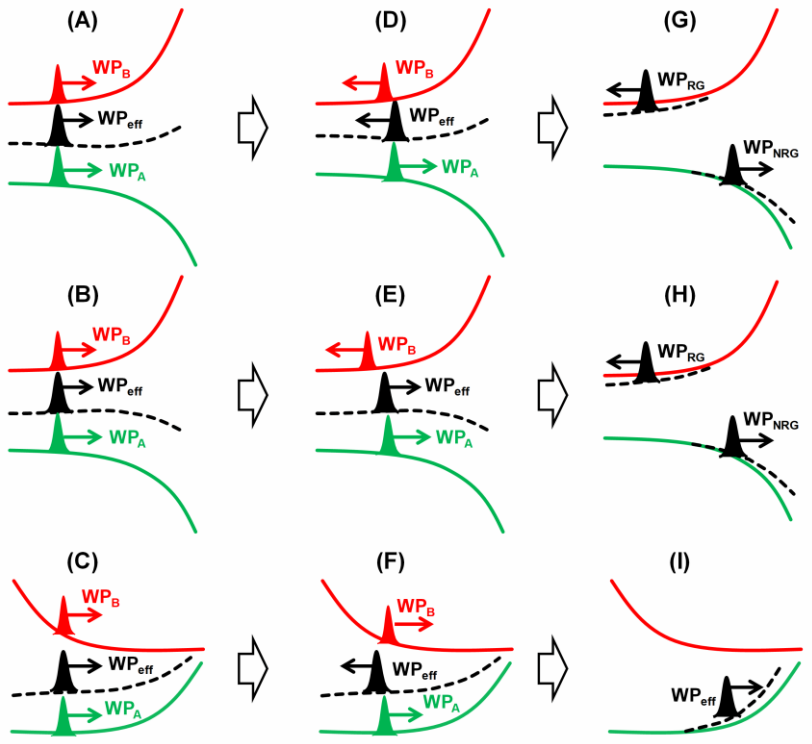

FIGURE 1. Schematic representation of (A, D, and G) the first, (B, E, and H) the second, and (C, F, and I) the third type of trajectory branching due to WP reflection using two-level systems as an illustration. In (A), (B), and (C), an effective WP (WP_{eff}) on the average PES (dashed line) well represents the WPs (WP_A and WP_B) on the two adiabatic PESs (green and red solid lines). In (D) and (E), WP_A continues moving on the lower PES while WP_B gets reflected on the upper PES. In these two cases, the reflected WP and the non-reflected WP should be described separately with two new effective WPs (i.e., WP_{RG} and WP_{NRG}) in (G) and (H). In (F), WP_{eff} becomes reflected while WP_A and WP_B do not. As shown in (I), the average PES is adjusted to make sure that the new effective WP can describe the energy-allowed WPs.

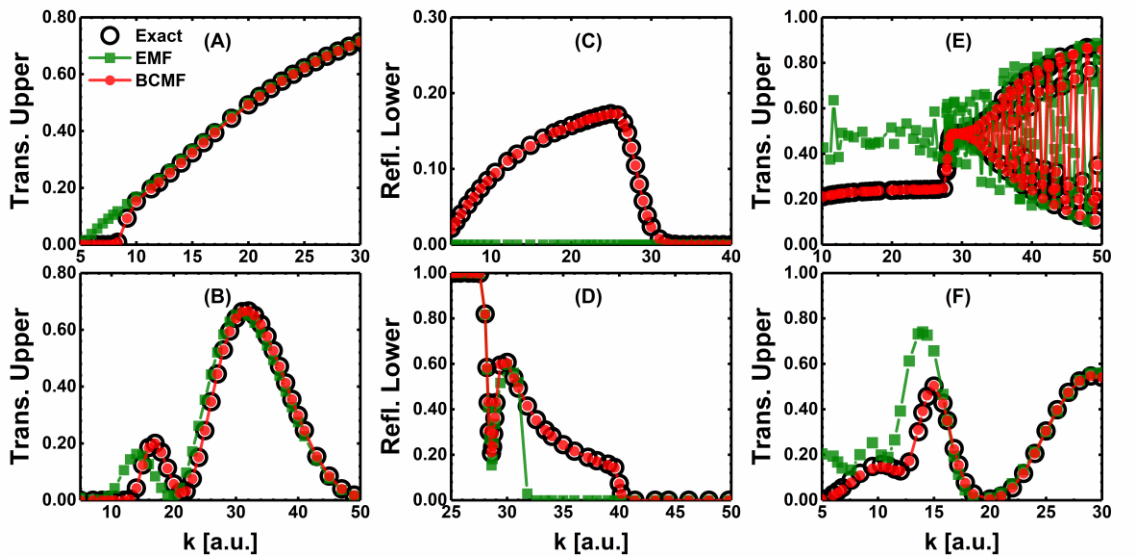

FIGURE 2. Transmission populations on the upper surfaces for (A) SAC and (B) DAC models, reflection populations on the lower surfaces for (C) ECR and (D) DBG models, and transmission populations on the upper surfaces for (E) DAG and (F) DRN models. Open circles are results obtained from exact quantum dynamics by DVR, while green solid squares and red solid circles represent the results of EMF and BCMF, respectively. The results of other channels are given in the SI.

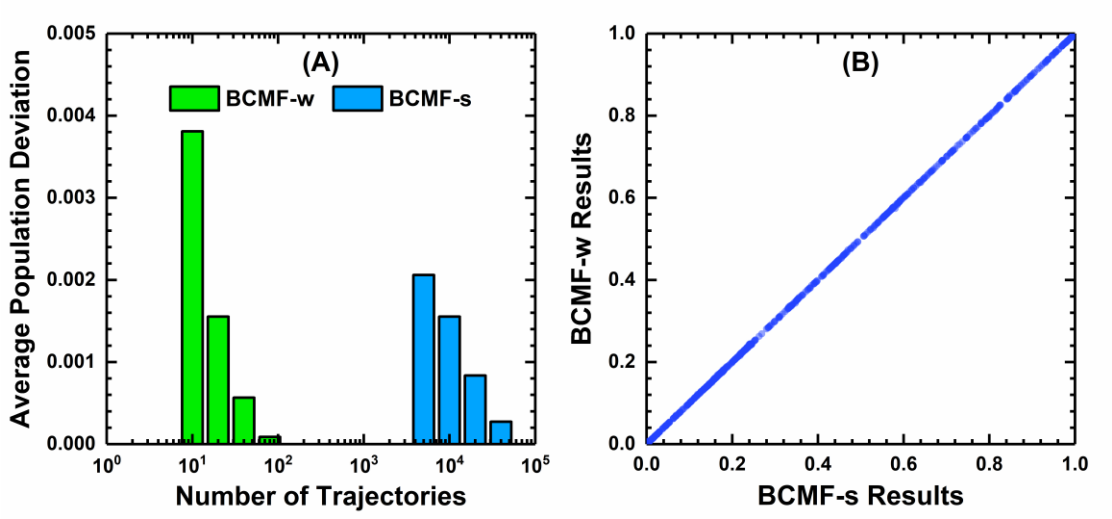

FIGURE 3. (A) Average population deviation with different number of trajectories with BCMF-w and BCMF-s algorithms, and (B) comparison of the individual channel populations. In (A), we set the maximum number of trajectories to 10, 20, 40, and 80 for BCMF-w, and different numbers of trajectories of 5000, 10000, 20000, and 40000 for BCMF-s. Calculations using 100 and 50000 trajectories are considered to get the converged results for BCMF-w and BCSH-s, respectively.

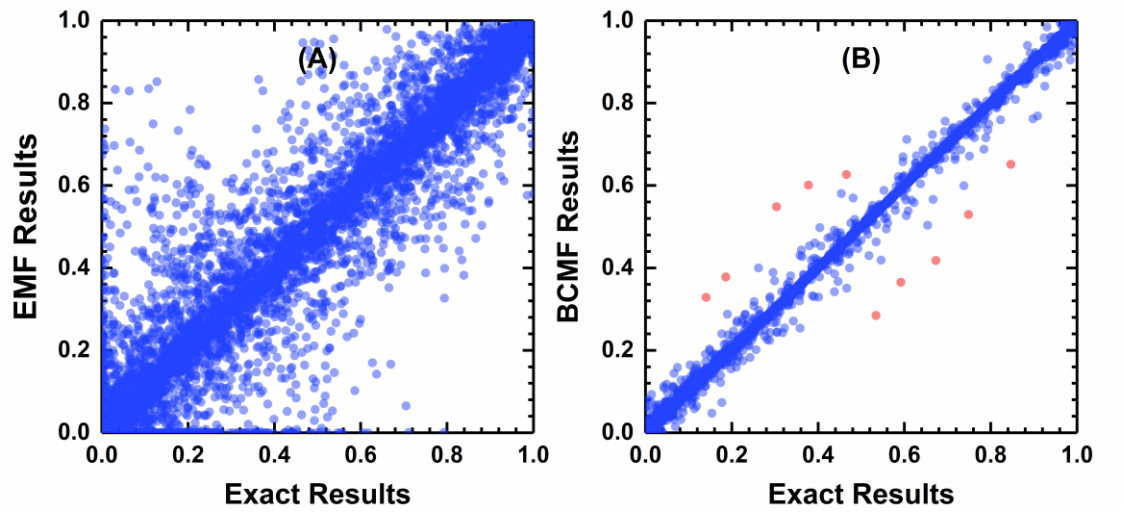

FIGURE 4. Comparison of the individual channel populations by the exact quantum dynamics by DVR and those by (A) EMF and (B) BCMF. We consider the model base containing 200 scattering models with 4 channels and 26 different initial nuclear momenta per model, and thus 20800 data points are shown in both (A) and (B). The red points highlighted in (B) belong to five calculations encountering strong nuclear quantum effects, that cannot be properly described by the initial Wigner sampling.

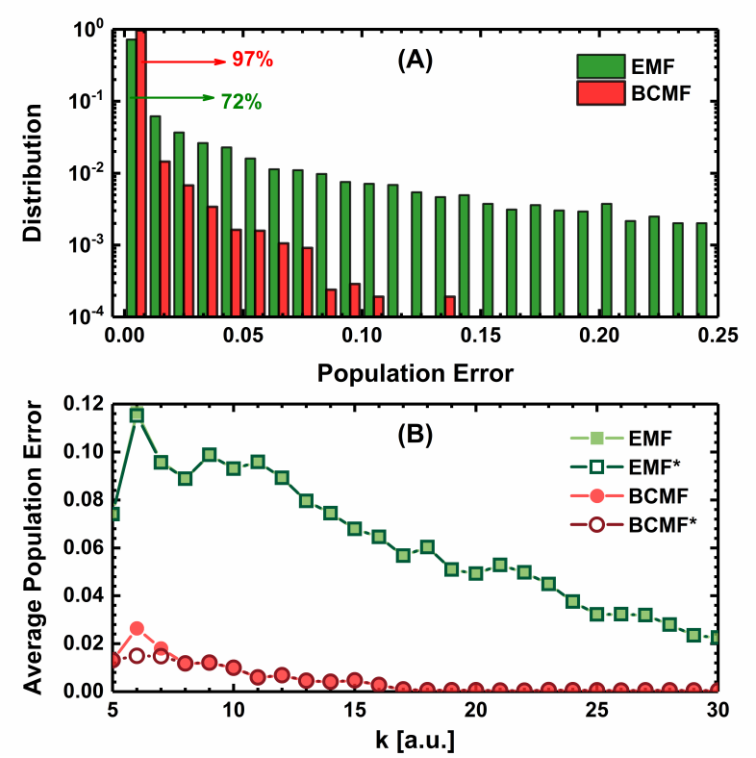

FIGURE 5. (A) Population error distribution of the EMF and BCMF methods as shown by green and red columns, respectively. For EMF, 72% of the data points show errors smaller than 0.01, while this value is increased to 97% in BCMF. (B) Average population error of different mean field approaches in the model base as a function of the initial nuclear momentum. The errors of EMF and BCMF are shown by light green solid squares and red solid circles, respectively. EMF* and BCMF* shown by open symbols represent results after excluding the data points featuring strong nuclear quantum effects as highlighted by red points in Fig. (4B).

REFERENCES

(1) Hammes-Schiffer, S.; Tully, J. C. Proton Transfer in Solution: Molecular Dynamics with Quantum Transitions. *J. Chem. Phys.* **1994**, *101*, 4657-4667.

(2) Song, K.; Shi, Q. Theoretical Study of Photoinduced Proton Coupled Electron Transfer Reaction Using the Non-Perturbative Hierarchical Equations of Motion Method. *J. Chem. Phys.* **2017**, *146*, 184108.

(3) Li, X.; Hu, D.; Xie, Y.; Lan, Z. Analysis of Trajectory Similarity and Configuration Similarity in On-The-Fly Surface-Hopping Simulation on Multi-Channel Nonadiabatic Photoisomerization Dynamics. *J. Chem. Phys.* **2018**, *149*, 244104.

(4) Zhang, T.-S.; Fang, Y.-G.; Song, X.-F.; Fang, W.-H.; Cui, G. Hydrogen-Bonding Interaction Regulates Photoisomerization of a Single-Bond-Rotation Locked Photoactive Yellow Protein Chromophore in Protein. *J. Phys. Chem. Lett.* **2020**, *11*, 2470-2476.

(5) Wang, L.; Beljonne, D. Flexible Surface Hopping Approach to Model the Crossover from Hopping to Band-Like Transport in Organic Crystals. *J. Phys. Chem. Lett.* **2013**, *4*, 1888-1894.

(6) Giannini, S.; Carof, A.; Blumberger, J. Crossover from Hopping to Band-Like Charge Transport in an Organic Semiconductor Model: Atomistic Nonadiabatic Molecular Dynamics Simulation. *J. Phys. Chem. Lett.* **2018**, *9*, 3116-3123.

(7) Caruso D.; Troisi, A. Long-Range Exciton Dissociation in Organic Solar Cells. *Proc. Natl. Acad. Sci.* **2012**, *109*, 13498-13502.

(8) Tu, Z.; Han, G.; Yi, Y. Barrier-Free Charge Separation Enabled by Electronic Polarization in High-Efficiency Non-Fullerene Organic Solar Cells. *J. Phys. Chem. Lett.* **2020**, *11*, 2585-2591.

(9) Peng, Q.; Yi, Y.; Shuai, Z.; Shao, J. Toward Quantitative Prediction of Molecular Fluorescence Quantum Efficiency: Role of Duschinsky Rotation. *J. Am. Chem. Soc.* **2007**, *129*, 9333-9339.

(10) Trivedi, D. J.; Wang, L.; Prezhdo, O. V. Auger-Mediated Electron Relaxation Is Robust to Deep Hole Traps: Time-Domain Ab Initio Study of CdSe Quantum Dots. *Nano Lett.* **2015**, *15*, 2086-2091.

(11) Ehrenfest, P. Bemerkung über die angenäherte Gültigkeit der klassischen Mechanik innerhalb der Quantenmechanik. *Z. Phys.* **1927**, *45*, 455-457.

(12) Tully, J. C. Molecular Dynamics with Electronic Transitions. *J. Chem. Phys.* **1990**, *93*, 1061-1071.

(13) Troisi, A. Charge Transport in High Mobility Molecular Semiconductors: Classical Models and New Theories. *Chem. Soc. Rev.* **2011**, *40*, 2347-2358.

(14) Tully, J. C. Perspective: Nonadiabatic Dynamics Theory. *J. Chem. Phys.* **2012**, *137*, 22A301.

(15) Wang, L.; Prezhdo, O. V.; Beljonne, D. Mixed Quantum-Classical Dynamics for Charge Transport in Organics. *Phys. Chem. Chem. Phys.* **2015**, *17*, 12395-12406.

(16) Wang, L.; Long, R.; Prezhdo, O. V. Time-Domain Ab Initio Modeling of Photoinduced Dynamics at Nanoscale Interfaces. *Annu. Rev. Phys. Chem.* **2015**, *66*, 549-579.

(17) Long, R.; Prezhdo, O. V.; Fang, W. Nonadiabatic Charge Dynamics in Novel Solar Cell Materials. *WIREs Comput. Mol. Sci.* **2017**, *7*, e1305.

(18) Crespo-Otero, R.; Barbatti, M. Recent Advances and Perspectives on Nonadiabatic Mixed Quantum-Classical Dynamics. *Chem. Rev.* **2018**, *118*, 7026-7068.

(19) Wang, L.; Qiu, J.; Bai, X.; Xu, J. Surface Hopping Methods for Nonadiabatic Dynamics in Extended Systems. *WIREs Comput. Mol. Sci.* **2020**, *10*, e1435.

(20) Nelson, T. R.; White, A. J.; Bjorgaard, J. A.; Sifain, A. E.; Zhang, Y.; Nebgen, B.; Fernandez-Alberti, S.; Mozyrsky, D.; Roitberg, A. E.; Tretiak, S. Non-Adiabatic Excited-State Molecular Dynamics: Theory and Applications for Modeling Photophysics in Extended Molecular Materials. *Chem. Rev.* **2020**, *120*, 2215-2287.

(21) Chen, H.-T.; Reichman, D. R. On the Accuracy of Surface Hopping Dynamics in Condensed Phase Non-Adiabatic Problems. *J. Chem. Phys.* **2016**, *144*, 094104.

(22) Peng, J.; Xie, Y.; Hu, D.; Lan, Z. Performance of Trajectory Surface Hopping Method in the Treatment of Ultrafast Intersystem Crossing Dynamics. *J. Chem. Phys.* **2019**, *150*, 164126.

(23) Parandekar, P. V.; Tully, J. C. Mixed Quantum-Classical Equilibrium. *J. Chem. Phys.* **2005**, *122*, 094102.

(24) Parandekar, P. V.; Tully, J. C. Detailed Balance in Ehrenfest Mixed Quantum-Classical Dynamics. *J. Chem. Theory Comput.* **2006**, *2*, 229-235.

(25) Sifain, A. E.; Wang, L.; Prezhdo, O. V. Mixed Quantum-Classical Equilibrium in Global Flux Surface Hopping. *J. Chem. Phys.* **2015**, *142*, 224102.

(26) Wang, L.; Beljonne, D. Charge Transport in Organic Semiconductors: Assessment of the Mean Field Theory in the Hopping Regime. *J. Chem. Phys.* **2013**, *139*, 064316.

(27) Carof, A.; Giannini, S.; Blumberger, J. How to Calculate Charge Mobility in Molecular Materials from Surface Hopping Non-Adiabatic Molecular Dynamics – Beyond the Hopping/Band Paradigm. *Phys. Chem. Chem. Phys.* **2019**, *21*, 26368-26386.

(28) Prodhan, S.; Qiu, J.; Ricci, M.; Roscioni, O. M.; Wang, L.; Beljonne, D. Design Rules to Maximize Charge-Carrier Mobility along Conjugated Polymer Chains. *J. Phys. Chem. Lett.* **2020**, *11*, 6519-6525.

(29) Subotnik, J. E.; Jain, A.; Landry, B.; Petit, A.; Ouyang, W.; Bellonzi, N. Understanding the Surface Hopping View of Electronic Transitions and Decoherence. *Annu. Rev. Phys. Chem.* **2016**, *67*, 387-417.

(30) Wang, L.; Akimov, A.; Prezhdo, O. V. Recent Progress in Surface Hopping: 2011-2015. *J. Phys. Chem. Lett.* **2016**, *7*, 2100-2112.

(31) Bittner, E. R.; Rossky, P. J. Quantum Decoherence in Mixed Quantum-Classical Systems: Nonadiabatic Processes. *J. Chem. Phys.* **1995**, *103*, 8130-8143.

(32) Schwartz, B. J.; Bittner, E. R.; Prezhdo, O. V.; Rossky, P. J. Quantum Decoherence and the Isotope Effect in Condensed Phase Nonadiabatic Molecular Dynamics Simulations. *J. Chem. Phys.* **1996**, *104*, 5942-5955.

(33) Prezhdo, O. V.; Rossky, P. J. Evaluation of Quantum Transition Rates from Quantum-Classical Molecular Dynamics Simulations. *J. Chem. Phys.* **1997**, *107*, 5863-5878.

(34) Zhu, C.; Jasper, A. W.; Truhlar, D. G. Non-Born-Oppenheimer Trajectories with

Self-Consistent Decay of Mixing. *J. Chem. Phys.* **2004**, *120*, 5543-5557.

(35) Zhu, C.; Nangia, S.; Jasper, A. W.; Truhlar, D. G. Coherent Switching with Decay of Mixing: An Improved Treatment of Electronic Coherence for Non-Born-Oppenheimer Trajectories. *J. Chem. Phys.* **2004**, *121*, 7658-7670.

(36) Granucci, G.; Persico, M. Critical Appraisal of the Fewest Switches Algorithm for Surface Hopping. *J. Chem. Phys.* **2007**, *126*, 134114.

(37) Granucci, G.; Persico, M.; Zoccante, A. Including Quantum Decoherence in Surface Hopping. *J. Chem. Phys.* **2010**, *133*, 134111.

(38) Shenvi, N.; Subotnik, J. E.; Yang, W. Simultaneous-Trajectory Surface Hopping: A Parameter-Free Algorithm for Implementing Decoherence in Nonadiabatic Dynamics. *J. Chem. Phys.* **2011**, *134*, 144102.

(39) Subotnik, J. E.; Shenvi, N. A New Approach to Decoherence and Momentum Rescaling in the Surface Hopping Algorithm. *J. Chem. Phys.* **2011**, *134*, 024105.

(40) Subotnik, J. E. Fewest-Switches Surface Hopping and Decoherence in Multiple Dimensions. *J. Phys. Chem. A* **2011**, *115*, 12083-12096.

(41) Jain, A.; Alguire, E.; Subotnik, J. E. An Efficient, Augmented Surface Hopping Algorithm That Includes Decoherence for Use in Large-Scale Simulations. *J. Chem. Theory Comput.* **2016**, *12*, 5256-5268.

(42) Xu, J.; Wang. L. Branching Corrected Surface Hopping: Resetting Wavefunction Coefficients Based on Judgement of Wave Packet Reflection. *J. Chem. Phys.* **2019**, *150*, 164101.

(43) Jaeger, H. M.; Fischer, S.; Prezhdo, O. V. Decoherence-Induced Surface Hopping. *J. Chem. Phys.* **2012**, *137*, 22A545.

(44) Shen, L.; Tang, D.; Xie, B.; Fang, W.-H. Quantum Trajectory Mean-Field Method for Nonadiabatic Dynamics in Photochemistry. *J. Phys. Chem. A* **2019**, *123*, 7337-7350.

(45) Heller, E. J. Time-Dependent Approach to Semiclassical Dynamics. *J. Chem. Phys.* **1975**, *62*, 1544-1555.

(46) Tully, J. C. Mixed Quantum-Classical Dynamics. *Faraday Discuss.* **1998**, *110*, 407-419.

(47) de Carvalho, F. F.; Bouduban, M. E. F.; Curchod, B. F. E.; Tavernelli, I. Nonadiabatic Molecular Dynamics Based on Trajectories. *Entropy* **2014**, *16*, 62-85.

(48) Kim, H.; Kapral, R. Nonadiabatic Quantum-Classical Reaction Rates with Quantum Equilibrium Structure. *J. Chem. Phys.* **2005**, *123*, 194108.

(49) Bai, S.; Xie, W.; Shi, Q. A New Trajectory Branching Approximation to Propagate the Mixed Quantum-Classical Liouville Equation. *J. Phys. Chem. A* **2014**, *118*, 9262-9271.

(50) Shenvi, N.; Subotnik, J. E.; Yang, W. Phase-Corrected Surface Hopping: Correcting the Phase Evolution of the Electronic Wavefunction. *J. Chem. Phys.* **2011**, *135*, 024101.

(51) Zhu, C. Restoring Electronic Coherence/Decoherence for a Trajectory-Based Nonadiabatic Molecular Dynamics. *Sci. Rep.* **2016**, *6*, 24198.

(52) Miller, W. H. Classical *S* Matrix: Numerical Application to Inelastic Collisions. *J. Chem. Phys.* **1970**, *53*, 3578-3587.

(53) Lee, H.-W. Theory and Application of the Quantum Phase-Space Distribution Functions. *Phys. Rep.* **1995**, *259*, 147-211.

(54) Colbert, D. T.; Miller, W. H. A Novel Discrete Variable Representation for Quantum Mechanical Reactive Scattering via the *S*-matrix Kohn Method. *J. Chem. Phys.* **1992**, *96*, 1982-1991.

(55) Manolopoulos, D. E. Derivation and Reflection Properties of a Transmission-Free Absorbing Potential. *J. Chem. Phys.* **2002**, *117*, 9552-9559.

(56) Martínez, T. J.; Ben-Nun, M.; Levine, R. D. Multi-Electronic-State Molecular Dynamics: A Wave Function Approach with Applications. *J. Phys. Chem.* **1996**, *100*, 7884-7895.

(57) Curchod, B. F. E; Martínez, T. J. Ab Initio Nonadiabatic Quantum Molecular Dynamics. *Chem. Rev.* **2018**, *118*, 3305-3336.

(58) Berry, M. V. Quantal Phase Factors Accompanying Adiabatic Changes. *Proc. R. Soc. Lond. A* **1984**, *392*, 45-57.

(59) Subotnik, J.; Miao, G.; Bellonzi, N.; Teh, H.-H; Dou, W. A Demonstration of Consistency between the Quantum Classical Liouville Equation and Berry's Phase and Curvature for the Case of Complex Hamiltonians. *J. Chem. Phys.* **2019**, *151*, 074113.

(60) Granucci, G.; Persico, M.; Toniolo, A. Direct Semiclassical Simulation of Photochemical Processes with Semiempirical Wave Functions. *J. Chem. Phys.* **2001**, *114*, 10608-10615.

(61) Fernandez-Alberti, S.; Roitberg, A. E.; Nelson, T.; Tretiak, S. Identification of Unavoided Crossings in Nonadiabatic Photoexcited Dynamics Involving Multiple Electronic States in Polyatomic Conjugated Molecules. *J. Chem. Phys.* **2012**, *137*, 014512.

(62) Wang, L.; Prezhdo, O. V. A Simple Solution to the Trivial Crossing Problem in Surface Hopping. *J. Phys. Chem. Lett.* **2014**, *5*, 713-719.

(63) Bai, X.; Qiu, J.; Wang, L. An Efficient Solution to the Decoherence Enhanced Trivial Crossing Problem in Surface Hopping. *J. Chem. Phys.* **2018**, *148*, 104106.

(64) Qiu, J.; Bai, X.; Wang, L. Crossing Classified and Corrected Fewest Switches Surface Hopping. *J. Phys. Chem. Lett.* **2018**, *9*, 4319-4325.

(65) Qiu, J.; Bai, X.; Wang, L. Subspace Surface Hopping with Size-Independent Dynamics. *J. Phys. Chem. Lett.* **2019**, *10*, 637-644.

(66) Liu, J. Recent Advances in the Linearized Semiclassical Initial Value Representation/Classical Wigner Model for the Thermal Correlation Function. *Int. J. Quantum Chem.* **2015**, *115*, 657-670.

(67) Shen, Y.; Wang, L. Semiclassical Moyal Dynamics. *J. Chem. Phys.* **2018**, *149*, 244113.

(68) Wang, L.; Sifain, A. E.; Prezhdo, O. V. Fewest Switches Surface Hopping in Liouville Space. *J. Phys. Chem. Lett.* **2015**, *6*, 3827-3833.

(69) Wang, L.; Sifain, A. E.; Prezhdo, O. V. Communication: Global Flux Surface Hopping in Liouville Space. *J. Chem. Phys.* **2015**, *143*, 191102.